Supporting Information

Hannezo et al. 10.1073/pnas.1312076111

SI Text

Morphologies of Planar Epithelial Cells

Derivation of the Effective Energy. For an hexagonal prism, $V=\frac{\sqrt{3}}{2}r^2h$, $\mathcal{A}_{basal}=\frac{\sqrt{3}}{2}r^2$, $\mathcal{A}_{lat}=2\sqrt{3}rh$, and $\mathcal{P}_{ap}=2\sqrt{3}r$. The total effective energy is then

$$F=\gamma_b\frac{\sqrt{3}}{2}r^2-\alpha_l 2\sqrt{3}rh+2\sqrt{3}\Lambda_a r+\frac{K}{2}\left(\frac{\sqrt{3}}{2}r^2h-V_0\right)^2+\frac{A}{h^2}+\frac{2A}{r^2}. \quad [S1]$$

or, if the volume is constant ($V=V_0$),

$$\mathcal{F}=\gamma_b\frac{\sqrt{3}}{2}r^2-4\alpha_l\frac{V_0}{r}+2\sqrt{3}\Lambda_a r+\frac{4Ar^4}{3V_0^2}+\frac{2A}{r^2}. \quad [S2]$$

Choosing $V_0^{1/3}$ as the unit length and $\frac{A}{V_0^{2/3}}$ as the unit energy, we obtain a dimensionless energy with only three effective parameters. Using nondimensional variables that we rename as $\frac{r}{(4/3)^{1/6}V_0^{1/3}}\to r$ and $\frac{\mathcal{F}V_0^{2/3}}{(3/4)^{1/3}A}\to\mathcal{F}$,

$$\mathcal{F}=\frac{\gamma_b V_0^{4/3}}{A}r^2-\frac{\alpha_l}{AV_0^{2/3}r}+\frac{\Lambda_a V_0}{A}r+r^4+\frac{2}{r^2}. \quad [S3]$$

And from the rescaling in the main text,

$$\mathcal{F}=\gamma_b r^2-\frac{\alpha_l}{r}+\Lambda_a r+r^4+\frac{2}{r^2}. \quad [S4]$$

Force Balance on a Cell. We first write the force balance in the vertical direction (Fig. S1), on the apical surface. The compressibility of the cell creates a pressure $K(V-V_0)$, so

$$\frac{2A}{h^3}-\alpha_l\mathcal{P}_{ap}+K(V-V_0)\mathcal{A}_{apical}=0, \quad [S5]$$

which is equivalent to $\frac{d\mathcal{F}}{dh}=0$.

We now write the force balance in the radial direction, on a lateral face of the prism:

$$\frac{4A}{r^3}-2\cos\left(\frac{\pi}{6}\right)\Lambda_a-\frac{\sqrt{3}r}{2}\gamma_b+K(V-V_0)\mathcal{A}_{lat}=0, \quad [S6]$$

which again is equivalent to $\frac{d\mathcal{F}}{dh}=0$.

Orders of Magnitude. Ref. 1 studies the confinement of actin fibers of physiological concentrations in emulsion droplets of radii varying between 5 μm and 50 μm. Because actin filaments have a persistence length of around 15 μm, confinement effects occur around these length scales and are monitored through microrheological measurements of the Plateau modulus G_0. This Plateau modulus is thus roughly constant for large sizes, before increasing drastically with confinement. The average value at the onset of confinement is of order $G_0=0.2$ Pa, which fixes an energy scale, for a cell of volume $V_0\approx10^{-15}\mathrm{m}^3$ (2), of $G_0V_0=2.10^{-16}$ J. This corresponds to a force of 1 nN exerted on a length scale of 200 nm, not far from the values forces exerted by cytoskeletal filament bundles in a cell.

Because the energy scale in our model is $\frac{A}{V_0^{2/3}}$, we make a rough estimation $A\approx10^{-24}\ \mathrm{J}\cdot\mathrm{m}^2$ in the main text.

Ref. 3 studies the rheology of *Xenopus* egg cytoplasmic extracts, which contain actin, microtubules, and intermediate filaments. Moreover, the extracts remains metabolically active, with reserves of ATP, and thus quite close to physiological conditions. The extract is shown to behave like a viscoelastic solid over timescales of several hours. The moduli measured are in the range $2-10$ Pa, always higher than that of the loss modulus, and therefore one order of magnitude larger than the moduli of actin filaments alone. Therefore, we estimated in the main text $A\approx10^{-24}-10^{-23}\ \mathrm{J}\cdot\mathrm{m}^2$.

Obviously, the mammalian epithelial cell is a more complex material. In particular, filaments can be bundled and aligned actively in vivo, which would decrease the energy necessary for confinement. In our model, this would translate to a homothetic increase of our parameters γ_b, α_l, and Λ_a. One could imagine a biochemical feedback of the nucleus compression on the values of the tensions, which could be hinted by experiments such as ref. 4, showing that a mechanical compression of the nucleus in endothelial cells caused a compaction of chromatin.

All these remarks reinforce the pertinence of drawing phase diagrams of cellular morphology: Although biological tissues can take not trivial paths on these phase diagrams, they are still bound to them, and the qualitative results we describe apply.

Critical Point. A critical point, defined as $\frac{d\mathcal{F}}{dr}=\frac{d^2\mathcal{F}}{dr^2}=\frac{d^3\mathcal{F}}{dr^3}=0$ (where two spinodals meet), separates regions of continuous and discontinuous morphological transitions. It is possible to get analytical limits for the coordinates of the critical point. If $\alpha_l\ll-1$, then the lateral tension is enough to stabilize cells to a nonzero base length, and the term $\frac{1}{r^2}$ in the energy becomes negligible. The condition $\frac{d\mathcal{F}}{dr}=\frac{d^2\mathcal{F}}{dr^2}=0$ can then be written as

$$2\gamma_b r+\frac{\alpha_l}{r^2}+\Lambda_a+4r^3=0 \quad [S7]$$

$$2\gamma_b-\frac{2\alpha_l}{r^3}+12r^2=0. \quad [S8]$$

As long as $\gamma_b<0$ and $|\gamma_b|\gg1$, there are two clear limits to Eq. **S8**: $r=\sqrt{\frac{-\gamma_b}{6}}$ and $r=\left(\frac{\alpha_l}{-\gamma_b}\right)^{1/3}$, which, respectively, yield in the (α_l,Λ_a) plane $\Lambda_a=\frac{4}{3\sqrt{6}}(-\gamma_b)^{3/2}$ and $\alpha_l=\frac{\Lambda_a^3}{27\gamma_b^2}$. One can check that this is indeed is a good approximation of the numerical solution (Fig. S4).

Moreover, the condition $\frac{d^3\mathcal{F}}{dr^3}=0$, under this approximation, leads to $r=\left(\frac{4}{\alpha_l}\right)^{1/5}$, and at the critical point, $\alpha_{lc}=\frac{1}{25\sqrt{10}}(-\gamma_b)^{5/2}$ and $\Lambda_{ac}=\sqrt{\frac{2}{5}}(-\gamma_b)^{3/2}$.

Cell Confinement and Phase Separation. We come back to the question of a tissue confined on a rigid substrate, with no division or apoptosis, for which no buckling is allowed. Considering N

identical cells and a total area A_0, there are no degrees of freedom: $r^2=\frac{A_0}{N}=r_0^2$. The total energy of the layer is then

$$\mathcal{E}=N\mathcal{F}(r_0). \quad \textbf{[S9]}$$

Nevertheless, we have seen that our mechanical equations lead to two possible cell aspect ratios. Therefore, the cells can minimize their total energy by phase separating into N_c columnar cells of area r_c^2 and N_s squamous cells of area r_s, such that $N=N_s+N_c$ and $A_0=N_s r_s^2+N_c r_c^2$. We define $n_s=\frac{N_s}{N}$ and $n_c=\frac{N_c}{N}$ as the fractions of squamous and columnar cells and $a_0=\frac{A_0}{N}$ as the average area accessible per cell.

The total energy is then

$$\mathcal{E}=N\left(n_s\mathcal{F}(r_s)+(1-n_s)\mathcal{F}\left(\frac{a_0-n_s r_s^2}{1-n_s}\right)\right). \quad \textbf{[S10]}$$

We minimize the energy from Eq. **S10** with respect to the two independent parameters r_s and n_s while varying the single relevant control parameter, a_0. In this problem, γ_b drops out of the total energy, because the basal area is constant. On the other hand, Λ_a and α_l control the onset of phase separation of the cells. As analyzed previously, high values of either Λ_a or α_l favor a bistable equilibrium. When squamous cells are more and more confined, their area uniformly decreases until a phase separation threshold, after which a mixture of columnar and squamous cells coexists Fig. S9*A*). Additional confinement does not change the morphology of either type of cell. Instead, the sheet accommodates the decreased area by converting squamous cells into columnar cells (a numerical calculation is given in Fig. S9*B*). For very high confinements, only columnar cells remain and are progressively squeezed additionally toward more and more columnar aspect ratios. For low values of Λ_a or α_l, no phase separation occurs, and the morphological transition is instead smooth (Fig. S9*C*). We numerically compute a phase diagram showing the region of phase separation (Fig. S9*D*).

Epithelial Sheet Bending

Derivation of the Energy for Tubes and Spheres. In the case of a cell curved in two directions (forming a sphere), we define the height h of a cell (we consider a cell as a section of a shell, so that the distance between apical and basal sides is h everywhere; Fig. S5), the side length of the apical surface r_1, and the side length of the basal surface r_2. To calculate the confinement energy of a columnar curved cell, we parameterize the characteristic radius of a cell at a height z as $r(z)=r_1+\frac{r_2-r_1}{h}z$. We integrate the confinement energy of slices of thickness dz:

$$\mathcal{E}_c=\frac{1}{h}\int_0^h\frac{2}{r(z)^2}dz=\frac{2}{r_1 r_2}. \quad \textbf{[S11]}$$

The confinement energy for the curved cell is thus approximately $\mathcal{E}_{conf}=\frac{1}{h^2}+\frac{2}{r_1 r_2}$. Moreover, the lateral area is then $h\frac{r_1+r_2}{2}$, the volume is $h\frac{r_1^2+r_2^2+r_1 r_2}{3}$, and the total energy for a cell is

$$\mathcal{F}_s=\frac{A}{h^2}+2\frac{A}{r_1 r_2}-\alpha_l h\frac{r_1+r_2}{2}+\gamma_b r_1^2+\Lambda_a r_2+K\left(h\frac{r_1^2+r_2^2+r_1 r_2}{3}-V_0\right)^2. \quad \textbf{[S12]}$$

If the cell volume is constant,

$$\mathcal{F}_s=-\frac{3\alpha_l}{2}\frac{r_1+r_2}{r_1^2+r_2^2+r_1 r_2}+\frac{A}{9}\left(r_1^2+r_2^2+r_1 r_2\right)^2+\frac{2A}{r_1 r_2}+\gamma_b r_1^2+\Lambda_a r_2. \quad \textbf{[S13]}$$

For a cell curved in one direction (forming a tube), the perimeter of the apical side is $\frac{r+r_2}{2}$, the basal area is $r_1 r$, the lateral area is $h\left(\frac{r}{2}+\frac{r_1+r_2}{4}\right)$, and the volume is $hr\frac{r_1+r_2}{2}$. The same calculation for the confinement energy yields a contribution $\frac{1}{r_1 r_2}$ in the curved direction and $\frac{1}{r^2}$ in the uncurved direction. The total energy is then

$$\mathcal{F}_c=-\frac{\alpha_l}{2}\left(\frac{1}{r}+\frac{2}{r_1+r_2}\right)+\frac{A}{4}r^2\left(r_1+r_2\right)^2+\frac{A}{r_1 r_2}+\frac{A}{r^2}+\gamma_b r_1 r+\Lambda_a\frac{r_2+r}{2}. \quad \textbf{[S14]}$$

In the case of an apical belt tension, and in the limit $\Lambda_a\gg\alpha_l$, the energies of the spherical and cylindrical morphologies F_s and F_c are

$$F_s\approx\frac{2}{r_1 r_2}+\frac{r_1^4}{9}+\Lambda_a r_2 \quad \textbf{[S15]}$$

$$F_c\approx\frac{1}{r_1 r_2}+\frac{1}{r^2}+\frac{r_1^2 r^2}{4}+\Lambda_a\frac{r+r_2}{2}. \quad \textbf{[S16]}$$

Minimizing each energy with respect to r_1, r_2 or r_1, r_2, r, the scaling of the spherical energy at equilibrium is $F_s\propto\Lambda_a^{4/9}$, whereas that of the cylindrical energy is $F_c\propto\Lambda_a^{2/3}$, in agreement with numerical integrations (Fig. S8*A*).

Finite Elasticity of the Substrate. In the previous sections, we analyzed two limiting cases of infinitely rigid substrate (planar sheets) and infinitely soft substrate (bended sheets). In general, however, the underlying substrate has a finite elasticity. In many events of epithelial sheet bending, the sheet rests on a thin placode (5). We model the substrate with a bending modulus K_p. This adds a new contribution to the energy (6), proportional to the basal area of a cell r_1^2:

$$F_{bend}=\left(\frac{K_p}{2}\mathcal{C}^2\right)r_1^2. \quad \textbf{[S17]}$$

The two limiting cases studied in the main text are $K_p\to\infty$ and $K_p\to 0$.

Of course, increasing the bending modulus of the stroma always decreases the spontaneous curvature of the epithelium. Fig. S6*B* displays a numerical integration for the same set of parameters as before: $\gamma_b=0$, $\alpha_l=4.5$, and $\Lambda_a=10$. Defining an effective bending modulus K_{eff} resisting the apical constriction, we find that K_{eff} is the sum of the effective modulus of the sheet described previously and the bending modulus of the stroma, as expected by putting two sheets in parallel: $K_{eff}=K_p+K_{sheet}$, where $K_{sheet}=\frac{\Lambda_a}{\mathcal{C}}$, given in Eq. **6** of the main text. Therefore, $K_{eff}\to K_p$, when $K_p\to\infty$, as expected, and K_{eff} converges to the same constant K_{sheet} as before when $K_p\to 0$. When exploring the full parameter space ($\gamma_b\neq 0$), we find additional complex behaviors (Fig. S6*C*).

Influence of the Cell–Substrate Tension γ_b on the Phase Diagram. We now consider the alternative case of an invagination driven by basal spreading ($\gamma_b\neq 0$ and $\Lambda_a\approx 0$). The topology of the phase

diagram (Fig. S7*B*) is different. Basal adhesion favors curved morphologies, lowering the effective bending stiffness of the sheet. As before, we derive scaling laws for large values of the basal adhesion ($\gamma_b < 0$ and $|\gamma_b| \gg \alpha_l$): $r_1 \propto \sqrt{-\gamma_b}$, $r_2 \propto -\gamma_b^{-1}$, and

$$\mathcal{C} \propto (-\gamma_b)^{5/2}. \quad \textbf{[S18]}$$

We now consider both apical belt tension and basal spreading. In the main text, we produce a phase diagram of 3D epithelial sheet morphology (Fig. S7).

For $\gamma_b = 0$ (Fig. S7 *A* and *B*), there is a zone of stability of quasi-flat sheets, around $\Lambda_a = 0$. These are sheets of squamous cells if $\alpha_l \ll 1$ and sheets of columnar cells if $\alpha_l \gg 1$ with a continuous transition between the two. When Λ_a increases, the spontaneous curvature of the epithelial sheet increases either continuously ($\alpha_l \ll 1$) or discontinuously ($\alpha_l \gg 1$), as we discuss in the main text.

When γ_b increases, this destabilizes flat sheets and causes the regions of stability of curved epithelial tissues to invade the phase diagram. A complex phase transition occurs: Two critical points first merge, and a region with three stable morphologies appears, when the third critical point merges with the other spinodals.

Sign of the Epithelial Curvature. In our model, the sign of the epithelial curvature can be either positive or negative. This depends on the relative values of the apical belt tension Λ_a and the basal tension γ_b.

To quantify this effect, we perform a numerical integration of the phase diagram of 3D architecture in the Λ_a, γ_b plane (Fig. S5*A*). We plot both the spinodal lines deliminating bistable equilibria regions and the line separating positive and negative curvatures. This separation is defined by the conditions $\frac{\partial \mathcal{F}}{\partial r_1} = \frac{\partial \mathcal{F}}{\partial r_2} = 0$ and $r_1 = r_2$.

As we show in Fig. S5*B*, the separation depends on the cell–cell lateral adhesion α_l. As α_l increases, the region of stability of negative curvatures shrinks.

For Λ_a and γ_b both positive, the confinement term $\frac{1}{h^2}$ is not needed to stabilize the shapes. Neglecting it, we can calculate analytically the separation line between positive and negative curvatures, which satisfies the equation

$$\alpha_l = 8\frac{\gamma_b}{\Lambda_a} - \frac{\Lambda_a^3}{2\gamma_b^2} \leq . \quad \textbf{[S19]}$$

This shows that indeed the solution α_l decreases monotonously with increasing Λ_a and increases monotonously with increasing γ_b. Moreover, on the zero-curvature line, $r_1 = r_2 = \frac{\Lambda_a}{2\gamma_b}$.

We also show a numerical solution for the basal and apical lengths for increasing apical belt tension Λ_a, for a given set a parameters (Fig. S5*C*).

Interestingly, studies on gastrulation in *Drosophila* (7) have shown that the transition from a concave to a convex epithelium is mediated by a relocalization of myosins from the basal side of the mesoderm to the apical side. In our formalism, this would mean that Λ_a increases as γ_b decreases.

Alternatively, if we consider an apical surface tension γ_a instead of an apical belt tension Λ_a, then our model is rigorously up–down symmetric, i.e., upon the substitution ($r_1 \to r_2$, $\gamma_b \to \gamma_a$). Then, the criterion for positive curvature is simply $\gamma_a > \gamma_b$ and for negative curvature is $\gamma_a < \gamma_b$.

Stability of Cellular Ellipsoid. We write, in analogy with the previous sections, the energy of a cell pictured in Fig. S8*B*, i.e., curved in two directions with two different curvatures $\mathcal{C}_1 = \frac{r_1 - r_2}{r_2 h}$ and $\mathcal{C}_2 = \frac{r_3 - r_4}{r_4 h}$. The volume of such a cell is $V = h\frac{2r_1r_3 + r_2r_3 + r_1r_4 + 2r_2r_4}{6}$, and the energy is

$$\mathcal{F}_e = \frac{1}{h^2} + \frac{1}{r_1 r_2} + \frac{1}{r_3 r_4} - \alpha_l h \frac{1}{2}\left(\frac{r_1 + r_2}{2} + \frac{r_3 + r_4}{2}\right) + \gamma_b r_1 r_3 + \gamma_a r_2 r_4 + K\left(V - 1\right)^2. \quad \textbf{[S20]}$$

If the cell volume is constant,

$$\mathcal{F}_e = \left(\frac{2r_1r_3 + r_2r_3 + r_1r_4 + 2r_2r_4}{6}\right)^2 + \frac{A}{r_1 r_2} + \frac{A}{r_3 r_4} - \frac{3\alpha_l}{2r_1r_3 + r_2r_3 + r_1r_4 + 2r_2r_4}\left(\frac{r_1 + r_2}{2} + \frac{r_3 + r_4}{2}\right) + \gamma_b r_1 r_3 + \gamma_a r_2 r_4. \quad \textbf{[S21]}$$

We confirm the stability analysis of cellular spheres vs. cellular tubes. The main difference is that the transition is no longer sharp, with a pitchfork supercritical bifurcation between a sphere (where the two curvatures are equal) and an elongated ellipsoid that approaches a tube (Fig. S8*C*). Nevertheless, infinite tubes are never stable in this model, because there is always a small curvature in the longitudinal direction.

Buckling Induced by Cell Shape Changes. As indicated in the main text, we parameterize the out-of-plane deformation of a buckled cell sheet by $l(z) = u\cos(qz)$, and the amplitude and wavelength u and q are such as to accommodate cells to their equilibrium height h_0 and average base length

$$r_0 = r\left(1 + \frac{u^2 q^2}{2}\right) \quad \textbf{[S22]}$$

in the regime of small curvatures $uq \ll 1$.

Nevertheless, in the buckled state, each cell is forced to adopt a spontaneous curvature, which is on average $\mathcal{C}_{sheet} = uq^2$ and has an energetic cost.

Therefore, one should compare the energetic cost of buckling and the energetic cost of cells not adopting their preferred height.

We define δr such that the elongated base length of a cell is $r_0 + \delta r$ and the shortened base length of a cell is $r_0 - \delta r$. The spontaneous curvature of a cell is $\mathcal{C}_{cell} = r_0 \delta r$ and has to be equal to the mean curvature of a sheet $\mathcal{C}_{sheet}$.

Combined with Eq. **S22**, this yields a relationship between the confinement $\Delta r = r_0 - r$ and the cell deformation δr:

$$\delta r = \sqrt{\frac{\alpha_l^3 \Delta r}{32}} q. \quad \textbf{[S23]}$$

The energetic cost in the buckled configuration can then be deduced from Eq. **S14**, with $r_1 = r_0 + \delta r$ and $r_2 = r_0 - \delta r$:

$$\mathcal{F}_{buck} = \frac{5}{3}\frac{\alpha_l^7}{4^6} q^2 \Delta r. \quad \textbf{[S24]}$$

Scaling Laws for a Generic Hard-Core Repulsion. We consider a more generic stabilizing energy of cytoskeleton confinement (or membrane confinement), $\mathcal{E}_{repuls} = \frac{1}{h^n} + \frac{2}{r^n} = r^{2n} + \frac{2}{r^n}$, to show that our qualitative results are unaffected by the assumption $n = 2$ we made in the main text.

We start by cells on rigid substrates. If cell–cell adhesion and actin belt contractility are small ($\alpha_l, \Lambda_a \ll |\gamma_b|$), cells are squamous

and spread to a base length $r \approx \left(\frac{-\gamma_b}{n}\right)^{1/(2n-2)} \gg 1$. If cell–cell adhesion is dominant ($\alpha_l \gg 1, |\gamma_b|$ and $\Lambda_a \approx 0$), cells are columnar and the stable base length is $r \approx \left(\frac{2n}{\alpha_l}\right)^{1/(n-1)} \ll 1$. If the apical belt is dominant ($\Lambda_a \gg 1$ and $\alpha_l \approx 0$), cells are columnar and the stable base length is $r \approx \left(\frac{2n}{\Lambda_a}\right)^{1/(n+1)} \ll 1$.

We plot in Fig. S2*A* the phase diagram of epithelial morphologies on flat substrates for various values of n, which we have chosen to correspond to various assumptions on the nature of confined polymers, to show that it still has the same topology.

In three dimensions, the scaling laws for the spontaneous curvature in the low Λ_a, high α_l regimes are not affected. Indeed, for any n, the scaling law for the spontaneous curvature is

$$\mathcal{C} \propto \frac{\Lambda_a}{\alpha_l^4 - 4n\alpha_l^{\frac{2n+2}{2n-1}}}, \qquad \text{[S25]}$$

and for any $n > 1$, in the limit $\alpha_l \gg 1$, $\alpha_l^4 \gg \alpha_l^{\frac{2n+2}{2n-1}}$. For the same reason, the scaling law for a small apical constriction is not affected. On the other hand, for an apical belt tension, in the high Λ_a regime,

$$\mathcal{C} \propto \Lambda_a^{\frac{8}{2n+5}}, \qquad \text{[S26]}$$

and for an apical surface tension, in the high γ_a regime,

$$\mathcal{C} \propto \gamma_a^{\frac{4}{n+5}}. \qquad \text{[S27]}$$

Again, we show the phase diagram of curved epithelia for a different value of n, to demonstrate that the main features remain unchanged. For $n = 4$ (Fig. S2*B*), there are still three spinodal tongues in the phase diagram for $\gamma_b = 0$, which merge for increasing values of γ_b.

We also plot for $n = 4$ the phase diagram of the stability of tubes vs. spheres, which again is not changed qualitatively (Fig. S2*C*).

Finally, even for these high-constriction regimes, there are some scaling laws that are completely generic. Notably, in both cases of belt tension and surface tension, the scaling law

$$r_1 \propto r_2^{-1/5} \qquad \text{[S28]}$$

holds for any n, which is again a strong prediction that could be tested experimentally.

Discussion of Different Hypotheses for the Stabilization of Cell Shape. In the main text, we proposed that the confinement of cytoplasmic components could be a mechanical cue that determines the morphology of epithelial cells, in concert with the active surface tensions from the apical, lateral, and basal sides. Obviously, alternative mechanisms of stabilization would be imaginable, for instance the active regulation of tensions to approach a target cellular shape, as discussed in ref. 8.

On flat substrates, we assume that cells have a preferred lateral area A_l^0 and a basal area A_b^0, and we expand the lateral and basal tensions, respectively, around these preferred areas:

$$\gamma_b = \gamma_b^0 + \delta_1\left(r^2 - A_b^0\right) \qquad \text{[S29]}$$

$$\alpha_l = \alpha_l^0 - \delta_2\left(\frac{V_0}{r} - A_l^0\right). \qquad \text{[S30]}$$

If δ_1 and δ_2 are positive, then the system is stable, and these stabilizing terms are exactly the same from a mathematical point of view as the ones described in the main text. The previous analysis then holds unchanged. In particular, this type of stabilizing mechanism gives rise to the same type of continuous vs. discontinuous transitions in cellular aspect ratios.

If δ_1 or δ_2 is negative, then the system is linearly unstable: One must expand the tensions up to the next order. Additional stable states are generically expected in this case.

For curved epithelia, the number of possible stabilizing terms is much larger. We fix $\gamma_b = 0$ in analogy to that in the main text, and we assume, as an example, an active regulation of the lateral adhesion α_l.

In analogy with the previous equations, we write the simplest dependence of α_l on A_{ap} and A_{bas}, which avoids $A_{bas} = r_1^2 \to 0$ and $A_{ap} = r_2^2 \to 0$,

$$\alpha_l = \alpha_l^0 - \delta_3\left(\frac{1}{A_{ap}} + \frac{1}{A_{bas}}\right), \qquad \text{[S31]}$$

and we incorporate, as in the main text, a term in $\frac{A}{h^2}$ in the energy to avoid $r_1 \to \infty$. We show that the main features of 3D architecture discussed in the main text are preserved using this assumption. Indeed, for low values of α_l, the curvature modulus of the sheet is low and the curvature increases smoothly with Λ_a. Moreover, α_l increases with increasing Λ_a (Fig. S3*A*). Above a critical value of α_l, the curvature modulus remains high until a critical value of Λ_a, above which it jumps to lower values. Interestingly, α_l undergoes the same type of continuous vs. discontinuous transitions as the geometrical parameters r_1 and r_2.

The phase diagram of epithelial cell morphology in 3D (Fig. S3*B*) is also similar to the one in the main text, with three spinodals joining for increasing values of γ_b. On the other hand, in this model, spheres are always favored compared with tubes, which may be related to the fact the effective lateral adhesion is lowered considerably (Fig. S3*A*) as Λ_a increases and r_2 decreases (α_l is always positive for large enough Λ_a; therefore, the hypothesis underlying the qualitative argument of the main text for tubular stability does not hold).

Experiments would be needed to verify whether the cellular morphology (for instance, the value of the apical and basal areas) has indeed a feedback effect on tensions.

1. Claessens MMAE, Tharmann R, Kroy K, Bausch AR (2006) Microstructure and viscoelasticity of confined semiflexible polymer networks. *Nat Phys* 2(3):186–189.
2. Kolahi KS, et al. (2009) Quantitative analysis of epithelial morphogenesis in Drosophila oogenesis: New insights based on morphometric analysis and mechanical modeling. *Dev Biol* 331(2):129–139.
3. Valentine MT, Perlman ZE, Mitchison TJ, Weitz DA (2005) Mechanical properties of Xenopus egg cytoplasmic extracts. *Biophys J* 88(1):680–689.
4. Versaevel M, Grevesse T, Gabriele S (2012) Spatial coordination between cell and nuclear shape within micropatterned endothelial cells. *Nat Commun* 3:671.
5. Borges RM, Lamers ML, Forti FL, Santos MFD, Yan CYI (2011) Rho signaling pathway and apical constriction in the early lens placode. *Genesis* 49(5):368–379.
6. Landau L, Lifchitz E (1970) *Theory of Elasticity*, A Course of Theoretical Physics (Pergamon, Oxford), Vol 7.
7. Dawes-Hoang RE, et al. (2005) Folded gastrulation, cell shape change and the control of myosin localization. *Development* 132(18):4165–4178.
8. Manning ML, Foty RA, Steinberg MS, Schoetz EM (2010) Coaction of intercellular adhesion and cortical tension specifies tissue surface tension. *Proc Natl Acad Sci USA* 107(28):12517–12522.

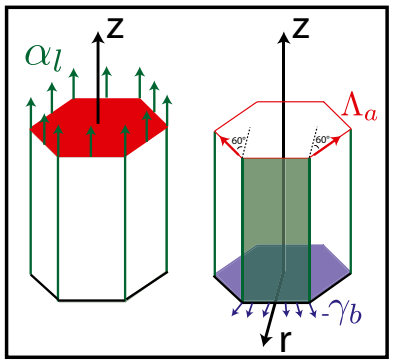

Fig. S1. Force balance on a cell.

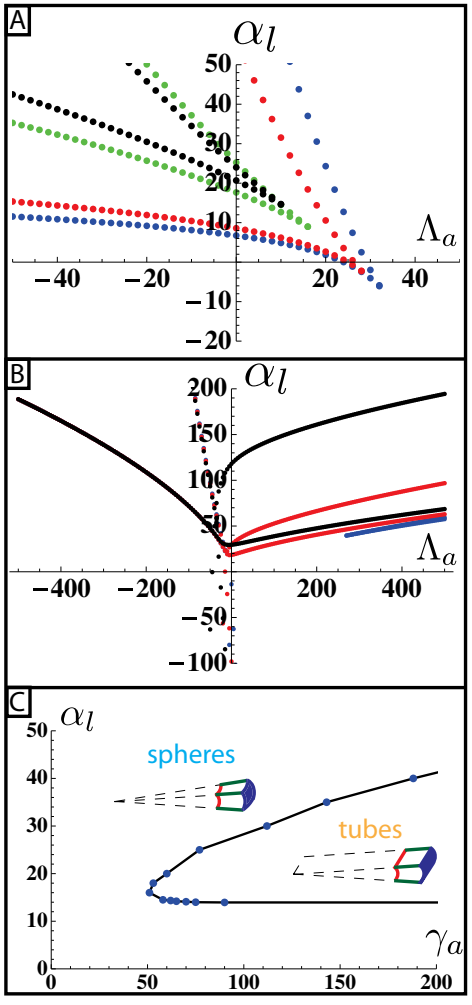

Fig. S2. Phase diagrams for various values of the exponent n of polymer repulsion. (*A*) Phase diagram of the 2D architecture of epithelial tissue on planar substrates, as a function of apical belt tension Λ_a and cell–cell adhesion α_l, for $\gamma_b = 15$ and $n = 2$ (blue), $n = 9/4$ (red), $n = 7/2$ (green), and $n = 4$ (black). (*B*) Evolution of the phase diagram of the 3D architecture of curved epithelia for $n = 4$ and for various values of $\gamma_b = 1$ (blue), $\gamma_b = 6$ (red), and $\gamma_b = 15$ (black). (*C*) Phase diagram of tubular vs. spherical organization of curved tissue, as a function of apical surface tension γ_a and cell–cell adhesion α_l, for $n = 4$.

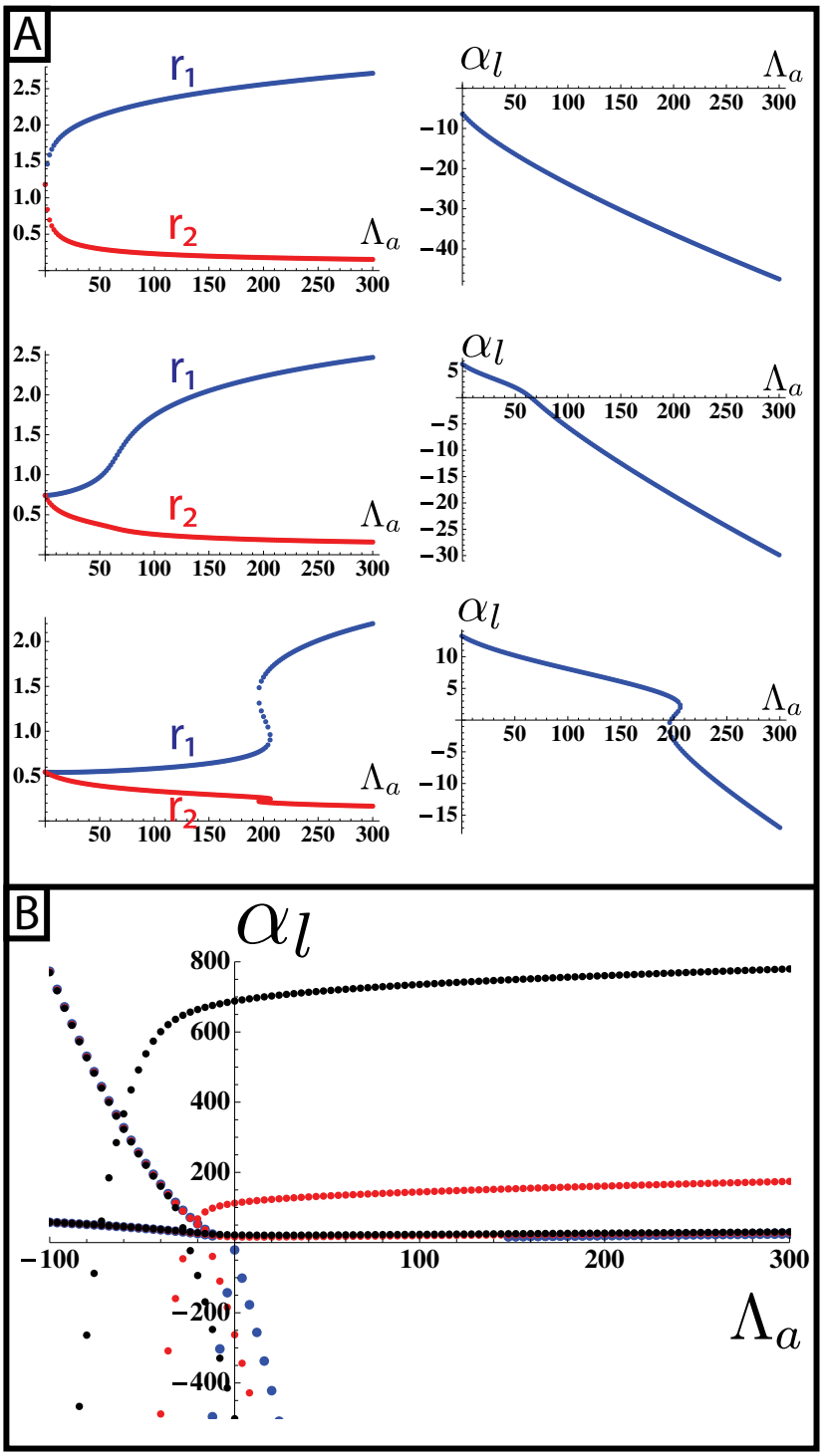

Fig. S3. A different hypothesis of shape stabilization: active regulation of the cell–cell tension. (*A*) (*Left*) Typical numerical integrations of the basal and apical lengths r_1 and r_2 as a function of apical belt tension Λ_a, for $\alpha_l = -5$ (*Top*), $\alpha_l = 10$ (*Middle*), and $\alpha_l = 20$ (*Bottom*). (*Right*) Corresponding cell–cell lateral tension, which now changes with Λ_a, because it is actively regulated depending on r_1 and r_2. We observe the same qualitative effect of cell–cell adhesion as in the main text. Moreover, α_l undergoes the same type of continuous vs. discontinuous transitions as the geometrical parameters r_1 and r_2. (*B*) Evolution of the phase diagram of the 3D architecture of curved epithelia for an active regulation of tensions and for various values of $\gamma_b = 0$ (blue), $\gamma_b = -5$ (red), and $\gamma_b = -15$ (black). Again, the qualitative results of the main text are unchanged.

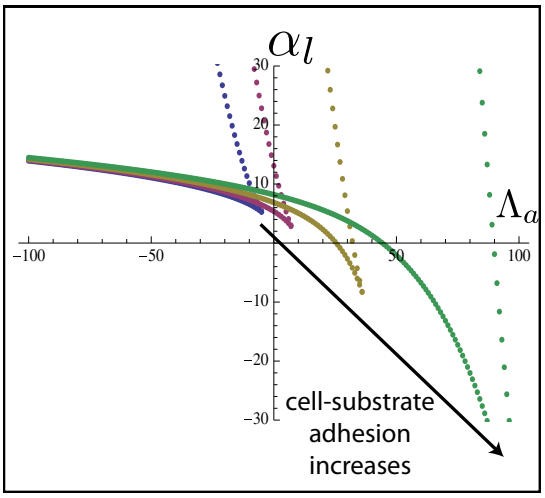

Fig. S4. Phase diagram as a function of Λ_a and α_l, for varying values of γ_b: 0 (blue), −5 (purple), −15 (brown), and −45 (green).

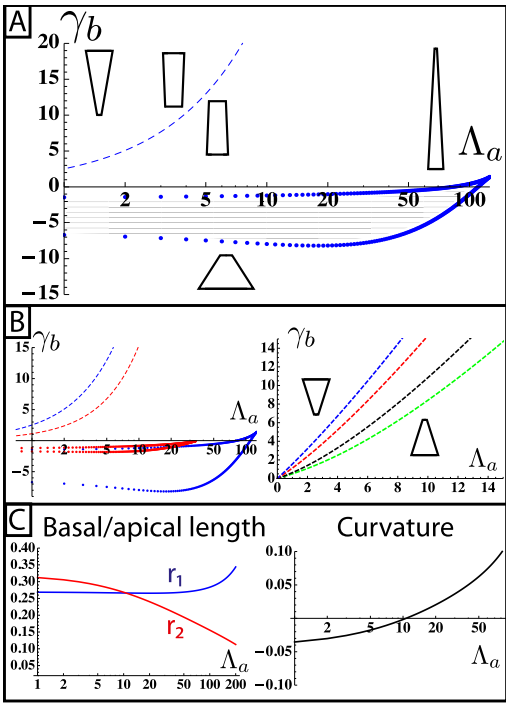

Fig. S5. (*A*) Phase diagram of the 3D architecture of epithelial tissue, as a function of apical belt tension force Λ_a and the basal tension γ_b. We plot both the spinodal lines (blue dots) deliminating bistable equilibria (hatched region) and the separation between negative and positive curvatures (dashed lines). Plot for $\alpha_l = 6$ is shown. (*B*) Same phase diagram of the 3D architecture comparing two values of cell–cell adhesion, $\alpha_l = 6$ (blue) and $\alpha_l = 4$ (red). Shown is a zoom-in on the frontier separating positive and negative curvature, for various values of cell–cell adhesion: $\alpha_l = -4$ (green), $\alpha_l = 0$ (black), $\alpha_l = 4$ (red), and $\alpha_l = 6$ (blue). (*C*) Example of a numerical integration of the basal and apical length (*Left*) and curvature changing sign (*Right*) for increasing Λ_a. We chose $\alpha_l = 6$ and $\gamma_b = 20$.

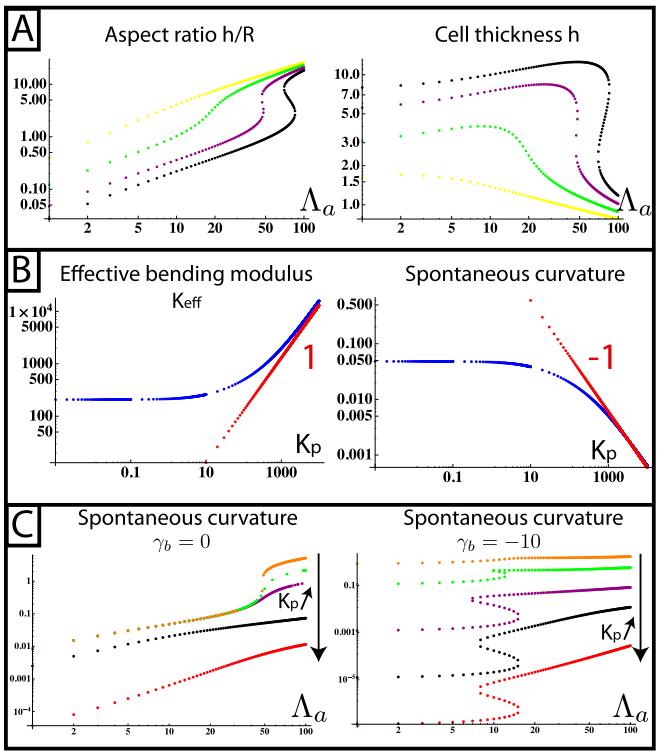

Fig. S6. (*A*) Limit of infinitely soft substrate: aspect ratio of the curved epithelia (height divided by the radius of curvature) and cell thickness, as a function of apical belt tension Λ_a, for various values of $\alpha_l = 1$ (yellow), $\alpha_l = 3$ (green), $\alpha_l = 4.5$ (purple), and $\alpha_l = 5.5$ (black). (*B*) For finite elasticities of the substrate, effective bending modulus and spontaneous curvature as a function of the substrate bending modulus K_p. We use the same parameter set as before: $\gamma_b = 0$, $\alpha_l = 4.5$, and $\Lambda_a = 10$. (*C*) Spontaneous curvature of an apically constricted tissue with various substrate bending moduli K_p and for $\alpha_l = 4.5$. (*Left*) $\gamma_b = 0$. For $K_p = 0$ (orange), the same transition as before is obtained. When K_p increases [$K_p = 0.01$ (green), $K_p = 0.1$ (violet), $K_p = 100$ (black), and $K_p = 10{,}000$ (red)], the curvature decreases as expected, and the discontinuous transition also disappears. (*Right*) $\gamma_b = -10$. When K_p increases[$K_p = 0.1$ (orange), $K_p = 1$ (green), $K_p = 100$ (violet), $K_p = 10^4$ (black), and $K_p = 10^6$ (red)], the curvature also decreases as expected. For $K \to \infty$, we expect to be in the previous limit of a planar epithelial, with a squamous to columnar morphological transition [observed for $K_p = 10^6$ (red)]. The discontinuous transition disappears when K_p decreases.

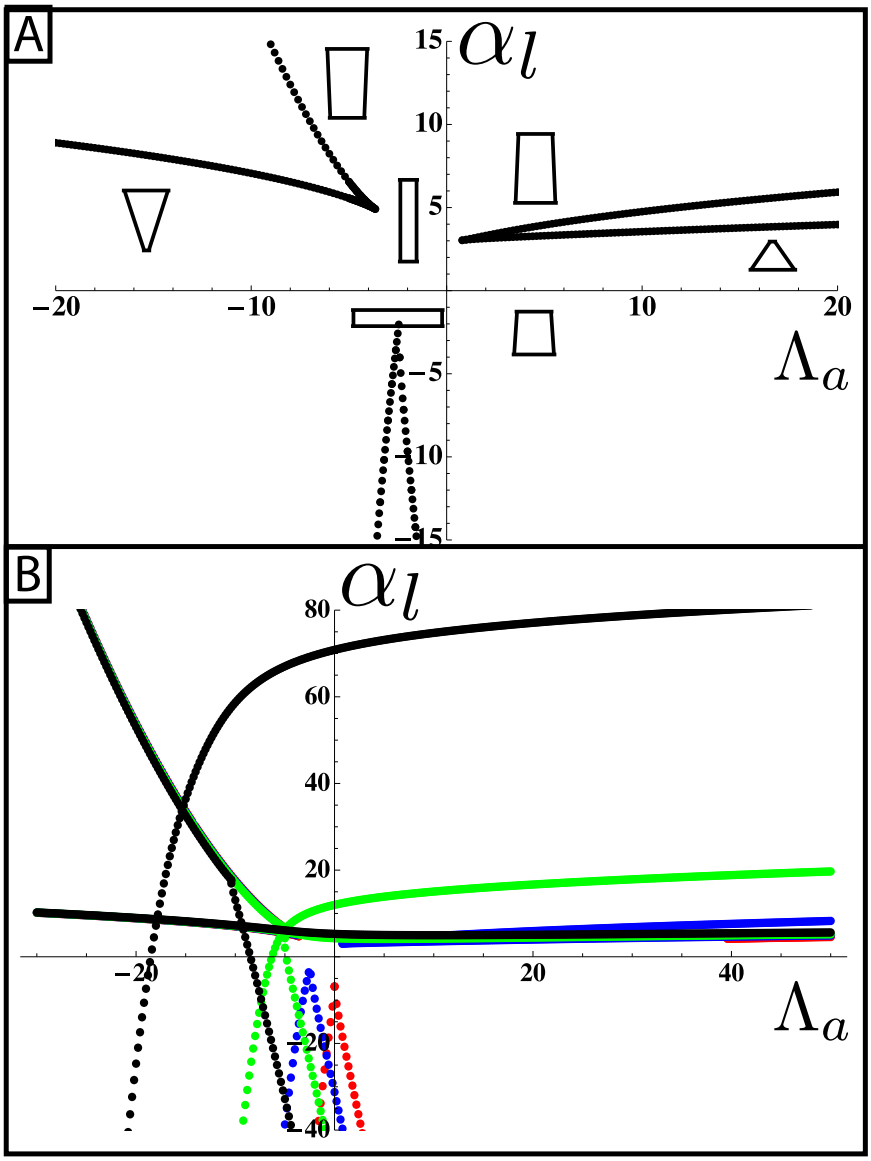

Fig. S7. (*A*) Phase diagram of the 3D architecture of epithelial tissue, as a function of apical belt tension Λ_a and cell–cell adhesion α_l, for $\gamma_b = -1$. (*B*) Evolution of the phase diagram for various values of $\gamma_b = 0$ (blue), $\gamma_b = -1$ (red), $\gamma_b = -2$ (green), and $\gamma_b = -4$ (black).

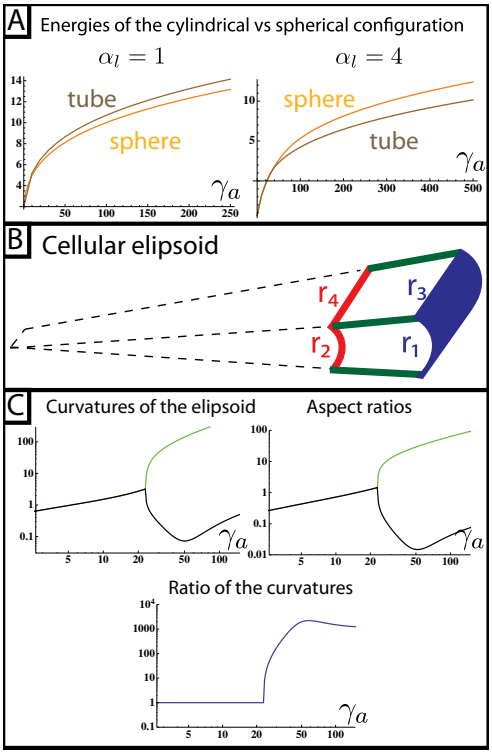

Fig. S8. Comparison of the mechanical stability for cellular tubes and spheres. (*A*) Energies of a sphere and tubes as a function of the apical cortex tension γ_a for $\alpha_l = 1$ (*Left*) and $\alpha_l = 4$ (*Right*). (*B*) Schematics of a infinitesimal piece of a cellular ellipsoid. (*C*) Curvatures ($\mathcal{C}_1$ and $\mathcal{C}_2$), aspect ratios ($h\mathcal{C}_1$ and $h\mathcal{C}_2$), and ratios of curvatures of an ellipsoid as a function of apical tension γ_a.

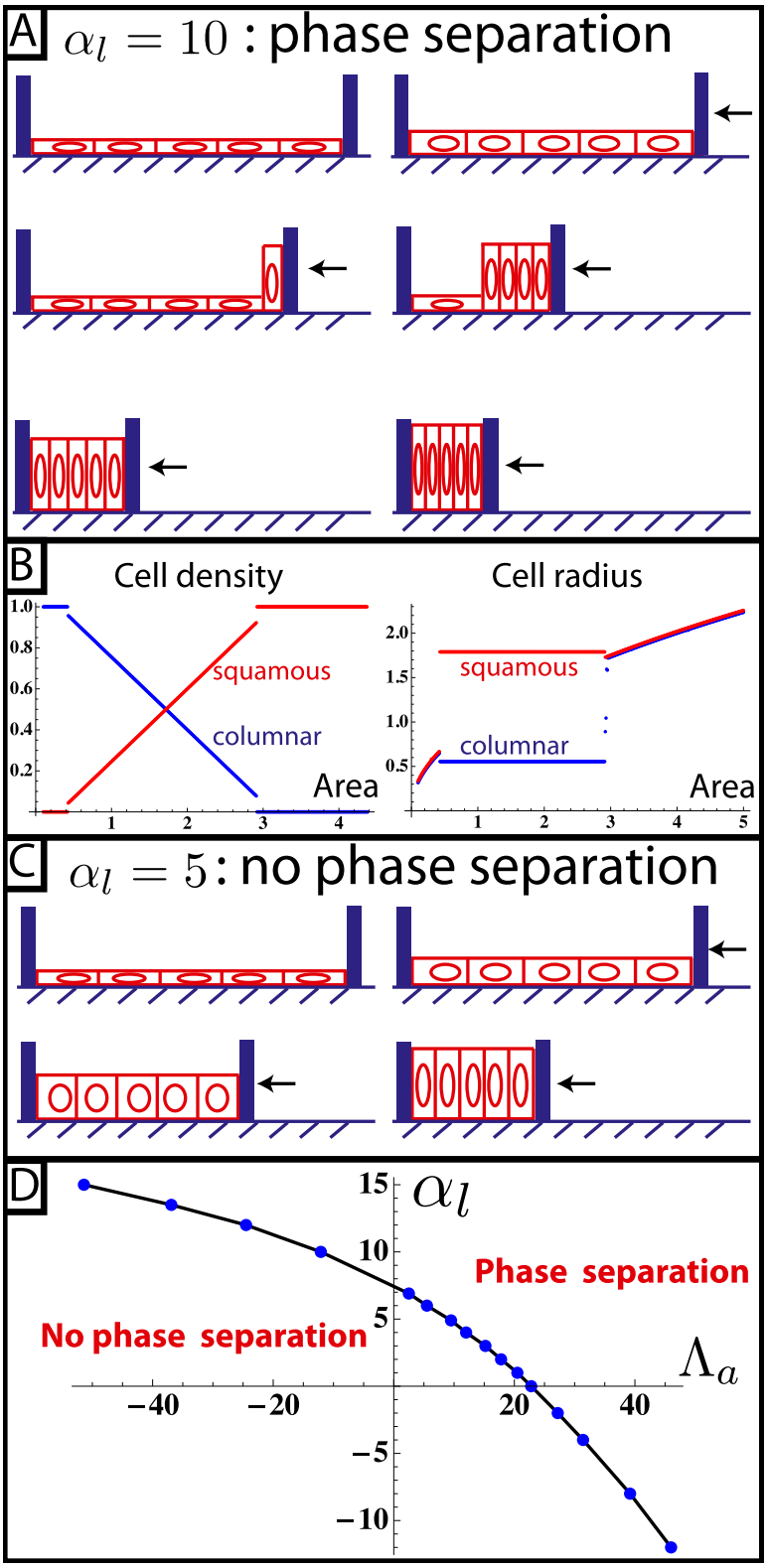

Fig. S9. Cell confinement and phase separation. When squamous cells are confined, two scenarios are possible. (*A* and *B*) For high values of cell–cell adhesions, a phase separation occurs (*A*), with squamous and columnar cells maintaining their radii and converting to match the total available area (*B*). (*C*) For low values of cell–cell adhesions, the transition is continuous. (*D*) Diagram of phase separation.